Lipidic Cubic Phase Crystal Structure of the Photosynthetic Reaction Centre from Rhodobacter sphaeroides at 2.35Å Resolution

ARTICLE *in* JOURNAL OF MOLECULAR BIOLOGY · SEPTEMBER 2003

Impact Factor: 4.33 · DOI: 10.1016/S0022-2836(03)00751-4 · Source: PubMed

doi:10.1016/S0022-2836(03)00751-4 J. Mol. Biol. (2003) 331, 681–692

JMB

Available online at www.sciencedirect.com

SCIENCE DIRECT®

Lipidic Cubic Phase Crystal Structure of the Photosynthetic Reaction Centre from *Rhodobacter sphaeroides* at 2.35 Å Resolution

Gergely Katona[1], Ulf Andréasson[2], Ehud M. Landau[3] Lars-Erik Andréasson[2] and Richard Neutze[1]*

[1]*Department of Molecular Biotechnology, Chalmers University of Technology, P.O. Box 462, SE-405 30 Gothenburg, Sweden*

[2]*Department of Biochemistry and Biophysics, Göteborg University, P.O. Box 462 SE-405 30 Gothenburg, Sweden*

[3]*Membrane Protein Laboratory Sealy Center for Structural Biology, and Department of Physiology and Biophysics University of Texas Medical Branch, Galveston, TX 77555-0437, USA*

**Corresponding author*

Well-ordered crystals of the bacterial photosynthetic reaction centre from *Rhodobacter sphaeroides* were grown from a lipidic cubic phase. Here, we report the type I crystal packing that results from this crystallisation medium, for which 3D crystals grow as stacked 2D crystals, and the reaction centre X-ray structure is refined to 2.35 Å resolution. In this crystal form, the location of the membrane bilayer could be assigned with confidence. A cardiolipin-binding site is found at the protein–protein interface within the membrane-spanning region, shedding light on the formation of crystal contacts within the membrane. A chloride-binding site was identified in the membrane-spanning region, which suggests a putative site for interaction with the light-harvesting complex I, the cytochrome bc_1 complex or PufX. Comparisons with the X-ray structures of this reaction centre deriving from detergent-based crystals are drawn, indicating that a slight compression occurs in this lipid-rich environment.

Keywords: bacterial photosynthetic reaction centre; X-ray crystallography; lipidic cubic phase crystallisation; membrane proteins; photosynthesis

Introduction

Photosynthetic bacterial reaction centres hold a place of honour within the field of membrane protein structural biology. The X-ray structure of the bacterial reaction centre of *Rhodopseudomonas viridis* represented the first integral membrane protein to be reported to high resolution,[1] and was followed shortly afterwards by that from *Rhodobacter sphaeroides*.[2] Since these pioneering studies a number of X-ray structures from bacterial photosynthetic reaction centres have been reported using detergent-based crystallisation protocols,[2–8] as well as X-ray structures in complex with cytochrome c_2.[9] Today, the resolution limit of detergent-based *R. sphaeroides* reaction centre crystals is 1.9 Å,[10] while for crystals of *R. viridis* the diffraction limit is 2.0 Å.[11] Structural differences between light and dark-adapted conformations have been reported.[7,10] Recent structural results from photosystem I[12] and photosystem II[13] from the thermophilic cyanobacterium *Synechococcus elongatus*, which (within conserved regions) shows a very similar fold and distribution of cofactors, add weight to the suggestion that a common evolutionary origin is shared by all reaction centres.[14]

Transmembrane regions of the bacterial reaction centre from *R. sphaeroides*[2] provide a scaffold for the non-covalent binding of four bacteriochlorophyll molecules, two bacteriopheophytins, two ubiquinone molecules and one non-heme iron atom, which are arranged symmetrically about an axis of 2-fold pseudo-symmetry.[1] Only one of two alternative branches is active in light-driven electron transfer across the cell membrane. The first light-driven electron transfer event from the special pair of chlorophyll molecules reduces a weakly bound quinone to a semi-quinone at the Q_B binding site. After a second light-driven electron transfer step, this is further reduced to quinol and (when coupled to proton uptake from

Abbreviations used: bR, bacteriorhodopsin; Q_A, and Q_B, primary and secondary quinone acceptors; Hepes, 2-[4-(2-hydroxyethyl)-1-piperazinyl]-ethanesulfonic acid; LDAO, lauryldimethylamine *N*-oxide.

E-mail address of the corresponding author: neutze@molbiotech.chalmers.se

the cytoplasm) exchanged with a fully oxidized quinone from the quinone/quinol pool. Since a dissociable quinone molecule is the terminal electron acceptor, the bacterial reaction centre from *R. sphaeroides* belongs to the family of type II reaction centres. A process of cyclic electron flow, *via* the cytochrome bc_1 complex and a soluble cytochrome c_2,[15] ensures the return of electrons to the special pair. The net result is that for each electron transfer cycle, two protons are transported from the cytoplasm to the periplasm.

Analogous to the reaction centres, bacteriorhodopsin (bR) is also a light-driven proton pump. This heptahelical retinal-binding protein was the first integral membrane protein from which any structural information was gleaned.[16] Nevertheless, it took a further 15 years until a high-resolution electron diffraction structure was reported.[17] Although detergent-based crystallisation experiments appeared promising,[18,19] it was not until the inception of a novel concept for membrane protein crystallisation in a lipidic cubic phase[20] that rapid and significant improvements in resolution emerged. High-resolution X-ray structures of the ground state[21,22] and the photointermediates of bR[23–29] followed, and in combination with lower-resolution electron microscopy structures of the later stages of the photocycle[30,31] have led to a self-consistent structural mechanism of vectorial proton transport by this model proton pump.[32] In addition, the ground-state structure of halorhodopsin,[33] and the ground-state structure[24,34] and an early intermediate structure[35] of sensory rhodopsin II, as well as that of sensory rhodopsin II in complex with its cognate transducer protein,[36] have been recovered to high resolution using lipidic cubic phase crystallisation.[20]

The generality of the lipidic cubic phase crystallisation concept was demonstrated by its successful application to the photosynthetic reaction centres from *R. viridis* and *R. sphaeroides*, as well as to the light-harvesting complex 2 from *Rhodopseudomonas acidophila*.[37] These crystals were small and did not allow high-resolution structural determination. Although detailed mechanistic information has emerged from X-ray structures of three members of the archaeal rhodopsin family, no high-resolution lipidic cubic phase structure has been reported from any other family of integral membrane proteins. In the current work, we grew 3D crystals of the bacterial reaction centre from *R. sphaeroides* and refined its X-ray structure to 2.35 Å resolution, reinforcing the general applicability of this crystallisation technique.[37] The crystal packing, as with all other lipidic cubic phase crystals to date,[24,33,34,36,38] displays a type I packing arrangement for which 3D crystals grow as multilayered 2D crystals. This is the first type I crystal packing reported for a reaction centre from a purple bacterium, and enables the location of the membrane bilayer within crystals to be assigned with confidence. In addition, a cardiolipin molecule is observed and is involved directly in forming crystal contacts within the membrane,

Table 1. Crystallographic data and refinement statistics

Resolution (Å)*	42.3–2.35 (2.43–2.35)			
No. unique reflections	51,199			
Completeness (%)	96.3 (97.6)			
Multiplicity[a]	7.2 (7.0)			
Mosaicity (deg.)	0.7			
$\langle I/\sigma \rangle$[a]	12.0 (2.8)			
R_{sym} (%)[a,b]	11.5 (66.8)			
R (%)[c]	21.4			
R_{free} (%)[c]	24.4			
r.m.s. bond length (Å)	0.007			
r.m.s. bond angles (deg.)	1.23			
No. atoms				
Protein	6386			
Waters	136			
Hetero	475			
Ramachandran plot[d]				
Most favored (%)	91.7			
Additionally allowed (%)	8.0			
Generously allowed (%)	0.3			
	Protein	Water	Hetero	Overall
Average B-factors (Å^2)				
Main-chain	39.37 ± 9.97			
Side-chain	40.37 ± 11.03			
All	39.98 ± 10.48	37.98 ± 8.11	39.82 ± 14.36	39.81 ± 10.75

[a] Values in parentheses indicate statistics for the highest resolution shell.
[b] $R_{sym} = \Sigma|I_o - \langle I \rangle I/\Sigma I_o \times 100\%$, where I_o is the observed intensity of a reflection and $\langle I \rangle$ is the average intensity obtained from multiple observations of symmetry-related reflections.
[c] R factor $= \Sigma||F_o| - |F_c||/\Sigma|F_o| \times 100\%$.
[d] By PROCHECK.

and a Cl^--binding site is identified. When compared with other structures of similar resolution determined from detergent-grown crystals, the transmembrane regions appear to be slightly compressed in this crystal form, possibly due to it being located within a lipid-rich environment.

Results and Discussion

Lipidic crystal structure of the reaction centre

Crystals of photosynthetic reaction centre from *R. sphaeroides* grown in the presence of monoolein (see Materials and Methods) diffracted to 2.35 Å resolution. These crystals belong to space group $P4_22_12$, with one molecule per asymmetric unit and the molecules are arranged within stacked anti-parallel planes. The structure was solved by molecular replacement using an X-ray structure from detergent-grown crystals (entry 1aij of the Protein Data Bank)[7] as a starting model (see Materials and Methods). X-ray diffraction data and final refinement statistics are summarized in Table 1. At the completion of refinement, the crystallographic *R* factor was 21.4%, with a free *R* factor of 24.4%, comparable with other reaction centre structures (Table 2).

The model exhibits well defined electron density almost throughout, except for a few side-chains of residues located in surface loops (e.g. L268, M13, M52, M188, H106, H118, H135, H197, and H220). Figure 1 illustrates the quality of the electron density map recovered at 2.35 Å resolution. Electron density for one of the two bacteriopheophytin cofactors is shown in Figure 1(a) with a hole at the centre of the unoccupied bacteriochlorin ring being clearly visible. Electron density for the fully occupied Q_A site is shown in Figure 1(b), and the conformation of the isoprenoid tail could easily be built and refined. In contrast, the electron density for the loosely bound quinone site (Q_B) did not enable a single conformation to be modelled with confidence. The ubiquinone molecule in the Q_B site is also usually poorly resolved in detergent-based crystal structures. The conformation of semi-quinone in the charge separated state differs significantly from ubiquinone in the charge neutral state, as was observed by Stowell *et al.*[7] and later by Fritzsch *et al.*[10] In addition to the remaining cofactors involved in electron transport, one non-heme iron atom, one lipid molecule, a chloride ion, and 136 water molecules were included in the final structure. The final ten residues of the H subunit were disordered.

Crystal packing

The packing arrangement of reaction centre molecules within the lipidic cubic phase grown crystals is shown in Figure 2(a). These crystals show a type I crystal form, in which the molecules are arranged in stacked 2D crystals, and every 2D bilayer is orientated anti-parallel to its adjacent bilayer. The solvent region is divided into lipidic and aqueous regions, where the lipidic region occupies the larger volume. A type I crystal packing has not been reported for any purple bacterial reaction centre. Extensive crystal contacts along the *c*-axis are mediated by interactions in the cytoplasmic region of the H-subunit, with additional contacts between the periplasmic regions of the L and M-subunits being visible, although these are considerably less extensive. Parallel with the *b*-axis, the strongest crystal contacts are again between the cytoplasmic domains of the H-subunits of adjacent molecules. In addition, crystal contacts are present within the plane of the membrane, with a lipid molecule (see below) mediating a salt-bridge contact between the membrane-membrane interfaces of two symmetry-related molecules. In contrast, there are no interactions within the plane of the membrane parallel with the *a*-axis, and the crystal contacts in this direction are mediated by the soluble domains of molecules in adjacent bilayers.

The packing arrangements of other lipidic cubic phase-grown membrane protein crystals are shown in Figure 2(b) and (c). In the cubic phase-generated crystals of bR (Figure 2(b), space group $P6_3$) all molecules are orientated vectorially along

Table 2. Comparison of this work and detergent based crystal structures used in the conformational analysis

PDB id	Resolution (Å)	Space group	*R*	R_{free}	Unit cell dimensions				Reference
					a (Å)	*b* (Å)	*c* (Å)	β (deg.)	
1aij	2.20	$P4_32_12$	0.216	0.270	140	140	272		7
1dv3	2.50	$P4_32_12$	0.226	0.252	141	141	275		4
1jgz	2.70	$P3_121$	0.215	0.249	141	141	187		70
1l9b	2.40	$P2_1$	0.220	0.264	78	116	80	110	9
1m3x	2.55	$P3_121$	0.185	0.209	141	141	187		6
1qov	2.10	$P3_121$	0.169	0.186	142	142	187		3
1e6d	2.30	$P3_121$	0.174	0.200	141	141	187		71
1pcr	2.65	$P3_121$	0.186	–[a]	141	141	187		72
	2.35	$P4_22_12$	0.214	0.244	100	100	237		This work

[a] Because of the lack of cross-validation information, a pessimistic estimate of $R_{free} = 0.240$ was used to calculate the uncertainties of atomic coordinates.

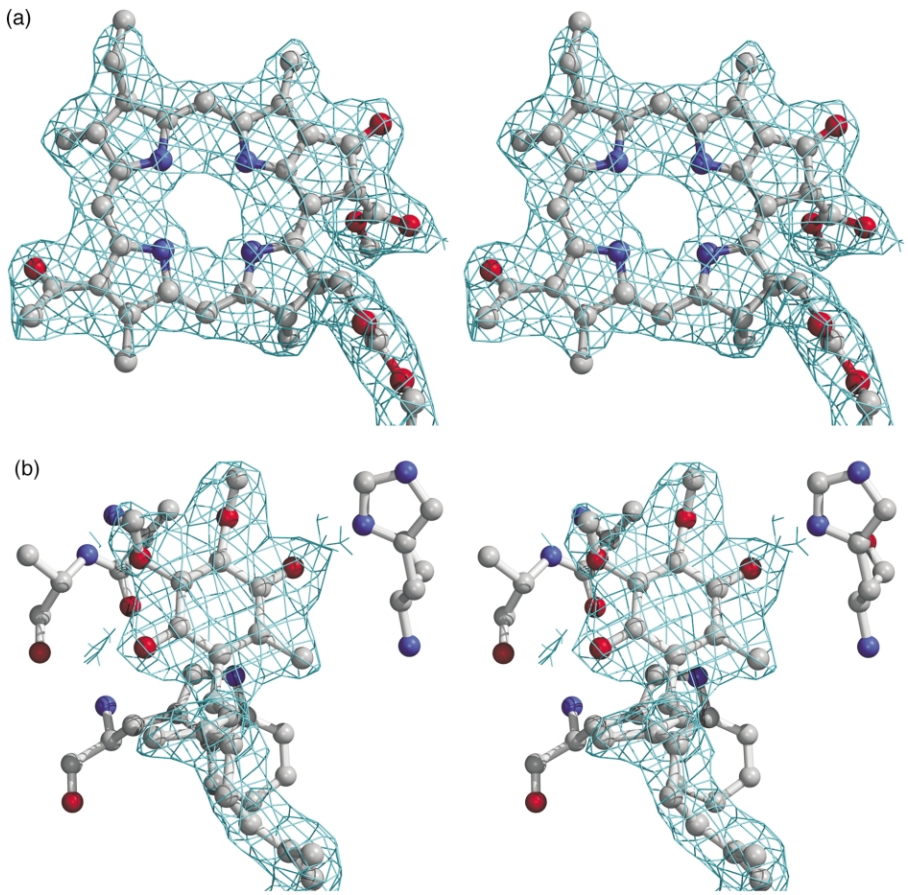

Figure 1. The $2mF_o - DF_c$ electron density map of selected cofactors: (a) bacteriopheophytin molecule; (b) ubiquinone molecule in the Q_A site. Both electron density maps are contoured at the 1σ level (σ is the root-mean-square electron density of the map).

the *c* direction.[38] Presumably because of the relatively weak contacts along this direction, this packing can lead to a stacking fault during crystal growth, and the crystals may become hemihedrally twinned.[39] For the pSRII cubic phase-grown crystal packing[24,34] (Figure 2(c), space group $C222_1$) the molecules exhibit alternate directionality within the plane, and hemihedral twinning is not possible. The crystal packing of halorhodopsin resembles that of bR, but with alternate directionality of the stacked bilayers (the space group is thus $P6_322$).[33] Evidently, while a type-I crystal packing appears to be a trade-mark of the lipidic-cubic phase crystallisation technique, there remains considerable variation within the packing. A mechanistic model for the crystallisation of bacteriorhodopsin from the lipidic cubic phase was proposed recently, whereby membrane proteins are thought to diffuse from curved lipid bilayers into patches of lower curvature, finally incorporating into planar lattices that associate to form highly ordered 3D crystals.[40]

Position and orientation of the membrane

An advantage of the type-I crystal packing is that the plane of the lipid-bilayer within crystals may be deduced easily. Monoolein (a C_{18} singly unsaturated lipid) naturally forms bilayers with varied curvatures, and has several other properties in common with biological membranes. The thickness of the hydrophobic part of the membrane is 34–35 Å at room temperature, which is in line with that of the cell membranes of *R. sphaeroides* excluding the polar head groups.[41] This may be expected, since the cell membranes of *R. sphaeroides* contain lipids whose apolar moiety comprises mainly vaccenic acid (11-*cis*-octadecenoic acid) lipids, which contain tails that are similar in size and structure to its isomer oleic acid (9-*cis*-octadecenoic acid).[42]

Although individual lipids, other than the cardiolipin molecule, could not be observed in the X-ray structure due to static or dynamic disorder, a trivial constraint of type I crystals is that each of the stacked 2D-crystals contains a single membrane bilayer. Since the 2D-crystals lie parallel with the *ab* plane of the unit cell, it is a powerful constraint to postulate that the plane of the membrane bilayer also lies parallel with the *ab* plane of the crystal. The height of this membrane bilayer can be reasoned (in order of decreasing importance) from: (i) the location of the hydrophilic domains of symmetry-related molecules (see Figure 2), which must be excluded from the

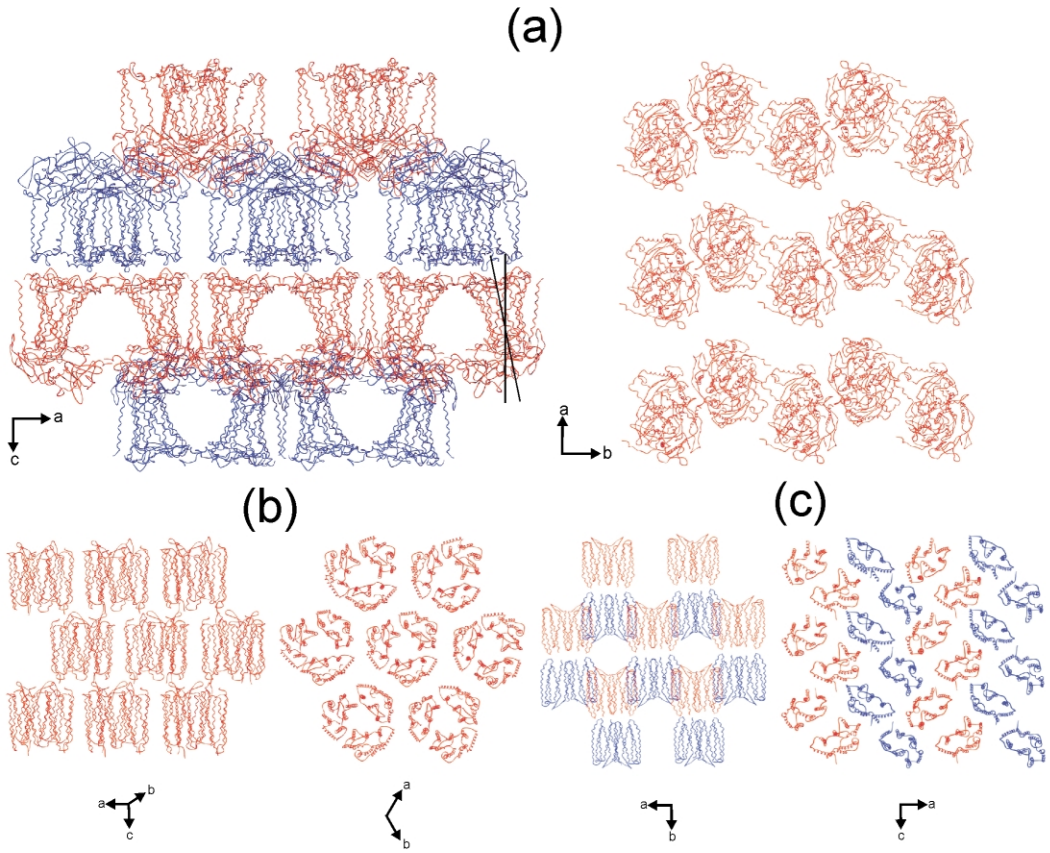

Figure 2. Packing arrangements of membrane proteins within lipidic cubic phase grown crystals: (a) *R. sphaeroides* reaction centre (this work). Left: the direction of view is parallel with the *ab* (membrane) plane. Right: the direction of view is parallel with the *c*-axis. (b) Bacteriorhodopsin crystal packing.[22] Left: the direction of view is parallel with the *ab* (membrane) plane. Right: the direction of view is parallel with the *c*-axis. (c) Sensory rhodopsin II crystal packing.[24] Left: the direction of view is parallel with the *ac* (membrane) plane. Right: the direction of view is parallel with the *b*-axis. The molecules are coloured (red or blue) to indicate their orientation (parallel or antiparallel) with respect to the normal of the plane of the membrane.

membrane bilayer; (ii) the thickness of monoolein bilayers, which was modelled as 34 Å; (iii) the length and positions of predicted hydrophobic α-helices; and (iv) the absence of putative water molecules within the membrane-spanning region.

Using these approximations, the most probable position for the membrane bilayer in the asymmetric unit is from 78 Å to 112 Å along the *c*-axis. The boundaries of the membrane are illustrated in Figure 3 (shown as transparent planes), which gives the location of the cofactors, the chloride ion and the cardiolipin molecule. From this assignment, it is observed that the 2-fold pseudo-symmetry axis of the reaction centre and the normal vector to the membrane plane (i.e. the *c*-axis) are inclined at an angle of 11.5° relative to each other, and the direction and extent of this tilt is illustrated in Figure 2(a). Since this tilt is (to a good approximation) within the mirror plane of pseudo-symmetry, it does not affect the heights (with respect to the boundaries of the membrane) of one quinone-binding site relative to the other, nor that of the other pseudo-symmetry-related cofactors. As such, this tilt of the reaction centre relative to the plane of the membrane appears unlikely to influence the uni-directionality of electron flow significantly.

The position and the thickness of the membrane spanning domain of the reaction centre of *R. sphaeroides* has been investigated using computational energy minimization techniques.[43] In contrast with the experimental orientation determined here, this computational work indicated that the 2-fold pseudo-symmetry axis of the reaction centre was parallel with the normal vector of the membrane plane[43] (i.e. the angle of inclination was estimated as $0(\pm 5)°$). It is possible that the discrepancy between the calculated and the observed tilt could be reconciled by including the closely bound cardiolipin molecule within the calculational model, since the position of the cardiolipin's head-group would impose additional constraints. As shown in Figure 3, even though the location of the cardiolipin molecule was not included in the above argument from which the membrane-spanning region was assigned, the predicted plane of the cytoplasmic boundary of the membrane bilayer just clips the charged phosphate head-group of this lipid.

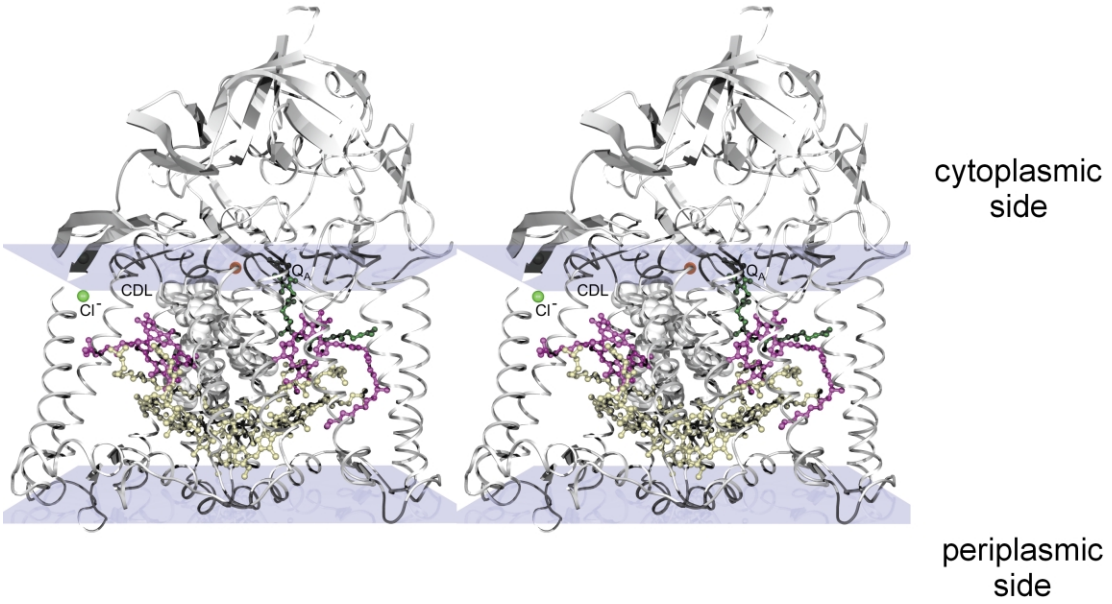

Figure 3. The arrangement of cofactors and the location of the membrane surface in the lipidic cubic phase-grown reaction centre structure. The cofactors are coloured as follows: yellow, bacteriochlorophyll; magenta, bacteriopheophytin; dark green, ubiquinone in the Q_A site; light green, Cl^-; orange, Fe^{2+}; gray space-filling model, cardiolipin molecule. The proposed membrane surfaces are indicated by light blue planes.

Lipid-mediated crystal contacts

As previously reported,[3] a cardiolipin molecule was identified that contacts the membrane-exposed surfaces of the H and M subunits. In this crystal packing, however, the same lipid's head-group forms an additional interaction with a loop of the L subunit of a symmetry-related molecule. Electron density for this lipid molecule is shown in Figure 4, and its location relative to the protein scaffold is illustrated in Figure 3. Lipid–protein interactions appear to play a stabilizing structural role, and have been suggested to influence the rate of electron transfer from cytochrome c_2 to the reaction centre's special pair.[44] In this case, only three out of four fatty acid chains could be identified within the electron density (Figure 4). The negatively charged head-group phosphatides of the cardiolipin molecule are stabilized by electrostatic interactions with the positively charged Lys144, His145 and Arg267 of subunit M, and Lys202 of the L-subunit of a symmetry-related molecule. In this manner, two symmetry-related molecules form strong crystal contacts at the membrane surface, forming a quasi-dimeric structure. Dimeric organisation of reaction centres was predicted for a membrane-bound environment on the basis of spectroscopic[45] and biochemical evidence.[46] PufX protein is considered mainly responsible for dimerisation,[47,48] but the involvement of cardiolipin

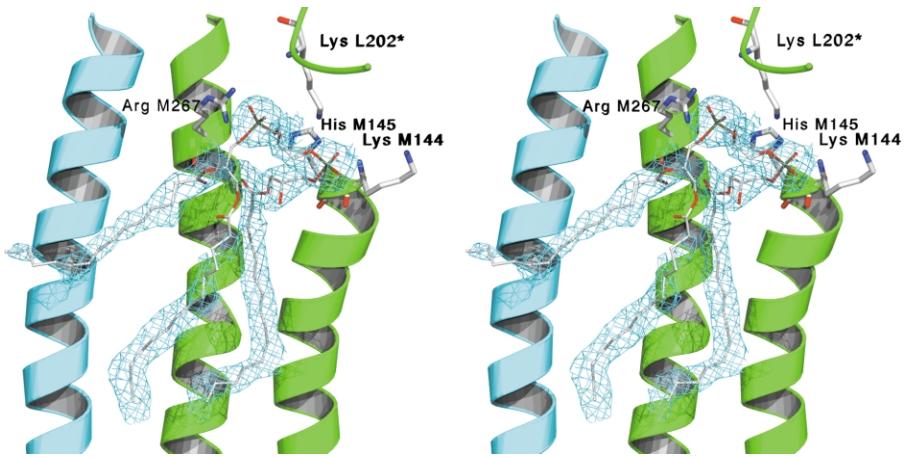

Figure 4. Electron density for a cardiolipin molecule involved in crystal contacts. This $2mF_o - DF_c$ electron density map is contoured at 0.7σ. Helices are coloured as follows: green, M subunit; cyan, H subunit. Lys L202 belongs to a symmetry-related molecule and forms a salt-bridge with the head group of the cardiolipin molecule.

molecules was predicted by modelling studies.[49] Our work supports the suggestion that a cardiolipin molecule could aid dimerisation.

In structures of other membrane proteins determined from lipidic cubic phase-grown crystals, several lipid molecules have been identified. For both bacteriorhodopsin[21,22] and halorhodopsin,[33] the biological lipids have been shown to be crucial in forming the natural trimers, and may mediate cooperative interactions between monomers. The current work, however, provides a unique example of protein–protein crystal contacts that are mediated directly by a negatively charged lipid head-group. As such, this observation appears to provide some rationale for the addition of charged lipid molecules as crystallisation additives.[24,34] It is noteworthy that a detergent molecule was identified to mediate crystal contacts in an *R. viridis* X-ray structure.[50] In that case, however, the contacts were between two H-subunits of symmetry-related molecules and the detergent tail did not appear to lie within the membrane-spanning region.

In addition to the above cardiolipin molecule, two other reaction centre lipid binding sites have been identified.[6] In this work, however, only faint traces of electron density could be found at their locations. An explanation for these differences might be that within a lipid bilayer structure, the lateral diffusion of lipid molecules is less restricted than within a detergent micelle. In the latter case, the hydrophobic nature of the fatty acid tails is likely to constrain lipid molecules near the protein's surface. With this argument in mind, the cardiolipin's head-group is bound strongly and the tail is confined tightly within a small cavity formed between two symmetry-related protein molecules, thereby yielding a relatively ordered environment.

Chloride ion

In Figure 5 an anion-binding site is identified, which was not observed previously in *R. sphaeroides* reaction centres, based upon the nearest-neighbour distances to two positively charged residues and the strength of the $F_o - F_c$ omit difference-Fourier map. This binding site, which is located just within the membrane-spanning region of the protein (green sphere in Figure 3), was too small to accommodate a sulphate or phosphate ion. Because the pH of the Hepes buffer was adjusted with hydrochloric acid, this site was assigned as a Cl^--binding site. Nearest-neighbour distances are 3.6 Å to Arg M132, 3.9 Å to Arg M136, 3.7 Å to the backbone nitrogen atom of Gly M53, and 3.6 Å to the backbone nitrogen atom of Gly M56. This site is somewhat reminiscent of the Cl^--binding site identified in the X-ray structure of sensory rhodopsin II,[24] which also lies just below the plane of the membrane and forms an ion pair with a positively charged arginine residue. In the detergent-based *R. viridis* reaction centre crystal structures (1prc and 1dxr), a sulfate ion is observed at a similar position even though the binding interactions are quite distinct, due to the limited conservation of residues in this region. In the detergent-based *R. sphaeroides* crystal structures, variable numbers of water molecules have been modelled in this Cl^--binding site (e.g. 1aij has three; 1e6d has two; 1pcr, 1m3x, 1jgz and 1dv3 have one; and 1qov and 1l9b have no water molecules). Another Cl^--binding site was suggested by Axelrod et al.,[4] although the assignment of this as a Cl^--binding site appears to be superceded, since it lies at a location occupied by the charged cardiolipin head-group (Figure 4).[3]

While the mechanistic significance of this Cl^--binding site is unclear, it is interesting to note that it lies close to a water channel connecting the mobile quinone (Q_B) binding site with the protein's surface. This Cl^--binding site is clearly pre-formed in the structure from detergent-grown crystal from which the above water-channel was first identified (PDB entry 1aij),[7] since, in that work, two water molecules were modelled into this site. Partial

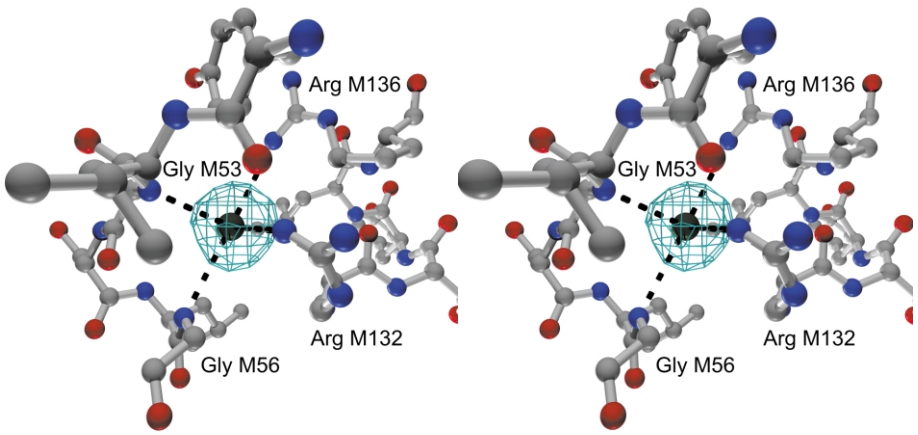

Figure 5. The $2mF_o - DF_c$ electron density of the putative Cl^- at the 1σ level. Arg M132, Arg M136, the backbone nitrogen atom of Gly M53 and the backbone nitrogen atom of Gly M56 are coordinating this ion as it binds.

compensation of the two positively charged arginine residues by an anion may be energetically favourable within the low-dielectric medium of the membrane.[51] A more speculative suggestion is that a cluster of charged side-chains located near the protein's surface but buried within the membrane could indicate specific sites for interaction with other integral membrane proteins. If true in this case, plausible candidates for such an interaction at this location are the photosynthetic antenna complex,[52] a closely associated cytochrome bc_1 complex of *R. sphaeriodes*,[52] or the PufX molecule.[47] The latter possibility receives circumstantial support from the fact that this Cl^--binding site lies adjacent to the entry/exit channel of the mobile quinone/quinol pocket.

Conformational changes

In addition to bacteriorhodopsin, this work provides a second example in which high-resolution X-ray structures of both detergent-grown crystals and lipidic cubic phase-grown crystals, may be compared. In the case of bacteriorhodopsin, the lower-resolution detergent crystal structure reported by Essen *et al.*[18] compares favourably with the higher-resolution structures recovered from a lipidic cubic phase-grown crystals[21,22] and there appear to be few systematic differences. To draw structural comparisons against the lipidic cubic phase structure refined here, six detergent-based X-ray structures of the reaction centre with similar resolution were first selected from the literature (Table 2, PDB codes: 1aij, 1qov, 1dv3, 1l9b, 1m3x, 1jgz). Prior to making any structural alignments, an error scaled difference distance matrix analysis was performed using the program ESCET.[53] Using this analysis, the conformationally invariant regions (i.e. error weighted internal distance changes of less than 2σ) within different reaction centre structures were identified and these regions were then used for the least-squares superposition of C^α atoms.

In Figure 6(a) the six structures from detergent-grown crystal (grey) are superimposed upon the structure from the lipidic cubic phase-grown crystal (cyan). This representation highlights the regions of the protein where the lipidic crystal structure differs from the ensemble of detergent-based crystal structures. In particular, it is observed that the regions where the lipidic structure is not obscured by the other structures (i.e. where cyan ribbons are visible) always indicate a slight offset towards the centre of the protein. The

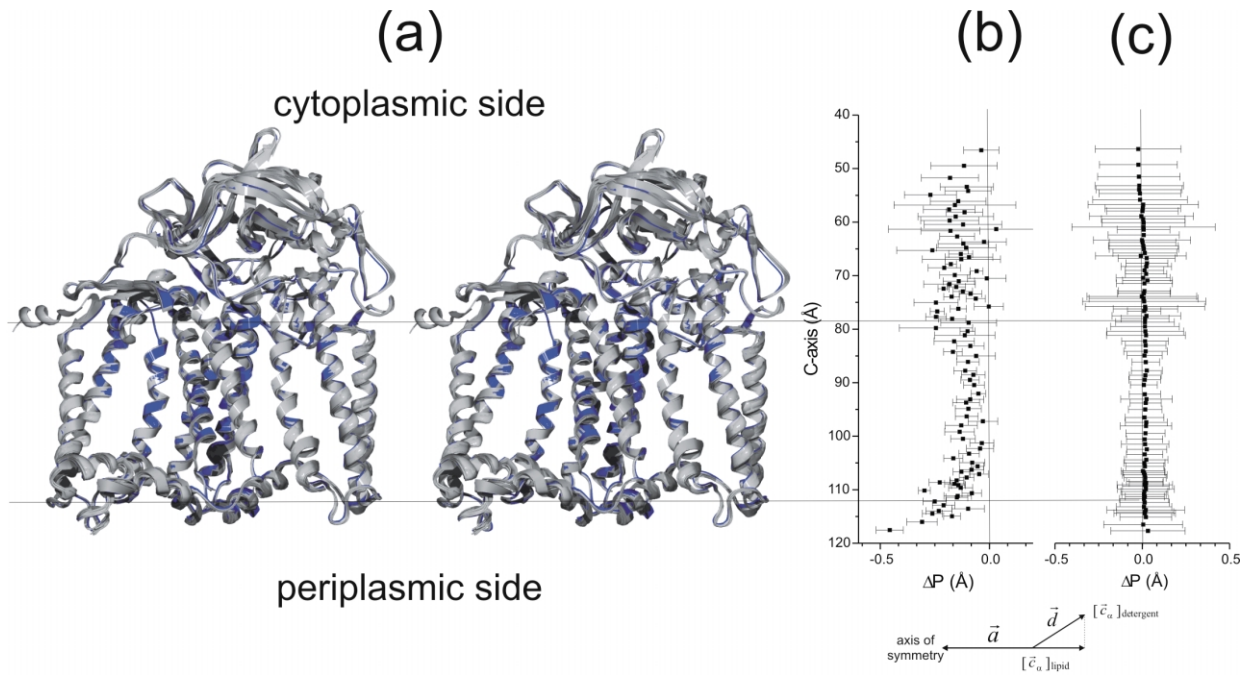

Figure 6. Structural comparisons of the lipidic cubic phase grown reaction centre structure against a selected set of structures determined from detergent-grown crystals. (a) Superposition of eight detergent-based crystal structures (grey) on the lipidic cubic phase crystal structure (blue). (b) Quantitative assessment of the compression of the lipidic cubic phase-grown structure relative to the detergent-based structures. Displacement vectors between the lipidic cubic phase and detergent-grown structures (calculated against C^α atoms) are projected onto the normalized vector lying parallel with the *ab* plane and pointing towards the axis of 2-fold pseudosymmetry. The average length of this projection vector, and its standard deviation, is plotted as a function of height along the crystallographic *c*-axis. A negative number means that the lipidic cubic phase-based structure's C^α atom is closer to the 2-fold pseudosymmetry axis than its corresponding value in the detergent structure. (c) A representation identical with that of (b), but instead of making the comparison against the C^α atoms of the lipidic cubic-based structure, the average position of the C^α atoms of the detergent structures are used for this comparison. As such, this calculation presents the underlying noise level associated with this representation.

transmembrane region most affected is the single transmembrane helix of the H-subunit, which is clearly offset towards the interior of the molecule in the lipidic phase structure. Nevertheless, this representation does not offer a quantitative description of these differences.

To quantify these structural differences we projected the difference vectors ($\mathbf{d} = [C^{\alpha}]_{detergent} - [C^{\alpha}]_{lipid}$) onto a unit vector pointing horizontally (i.e. parallel with the *ab* plane) towards the internal pseudo symmetry axis (**a**, these vectors are illustrated in Figure 6(b), bottom right). The average magnitudes of the resulting projection (compression) vectors are shown as a function of the height of C^{α} relative to the membrane in Figure 6(b), with error bars indicating the standard deviation of these changes relative to the six structures against which the comparisons are drawn. Figure 6(c) shows a plot that is identical with that given in Figure 6(b), but instead of using the lipidic crystal structure for comparison, the average of all detergent structures was used (i.e. $\mathbf{d} = [C^{\alpha}]_{detergent} - [C^{\alpha}]_{average}$) illustrating the noise level of this representation. Whereas the projected differences are distributed symmetrically about $\Delta P = \mathbf{d}\cdot\mathbf{a} = 0$ in Figure 6(c), the same distribution is skewed towards $\Delta P < 0$ for all C^{α} atoms in Figure 6(b). This indicates that in the lipidic X-ray structure, the protein has become slightly compressed towards the axis of pseudo-symmetry.

It is interesting to note that it is the H-subunit (on the cytoplasmic side) that shows the greatest degree of heterogeneity, even from one detergent structure to another (i.e. error bars are larger in this region in Figure 6(c)). On the other hand, while for the L and M subunits the magnitudes of these differences are not as pronounced, the conformational changes are considerably more homogeneous. A rational explanation for these observations appears to be that most crystal contacts are made through the hydrophilic domains (i.e. primarily the H-subunit). Since crystal contacts can vary considerably from one space group to another, even the detergent-based structures show significant heterogeneity in this region. In contrast, the membrane-spanning region is relatively unaffected by crystal contacts; rather, it is structurally perturbed by interactions with the surrounding detergent and lipid molecules. It is plausible that the partial pressure of the lipidic bilayer environment in lipid-rich type I crystals leads to a slight compression of the entire transmembrane spanning region relative to the detergent structures. Surface pressure in membranes is believed to have a stabilizing effect on the structural integrity of the entire system.[20,54] Structural effects were observed also on reaction centres in Langmuir–Blodgett films upon changes of surface pressure,[54] with the protein denaturing at low partial pressures and reorienting relative to the plane of the membrane at intermediate partial pressures. Moreover, the close packing in membrane systems may contribute to the thermal stability of the proteins.[55]

Conclusions

This work realizes the potential of lipidic cubic phase crystallisation for structural studies of the photosynthetic reaction centre from *R. sphaeroides* and sheds light on the influence of the membrane bilayer on membrane protein structure. Considering that lipidic cubic phase crystallisation[20] led to rapid and significant improvements in the diffraction power of bacteriorhodopsin crystals over more conventional detergent crystallisation techniques,[32] it is anticipated that further improvements in resolution are possible. While the lipidic cubic crystals of reaction centres have not reached the diffraction limit of detergent-based crystals (2.1 Å[3] and 2.0 Å[11] resolution, respectively), the optical properties of thin and still well-diffracting crystals could be advantageous for many applications. A clear advantage of lipid-rich crystals is that the membrane bilayer can be identified within the crystal structure with a high degree of confidence. In this context, the 2-fold symmetry axis of the molecule is somewhat tilted relative to the plane of the membrane, in contrast with earlier estimates using energy minimization techniques. It is curious that a cardiolipin molecule, previously observed in another crystal structure[3] mediates an important crystal contact between two symmetry-related molecules in this crystal form. The importance of lipid molecules in forming crystal contacts may yet prove general as more X-ray structures from lipid-rich environments emerge. In addition, the observation of a chloride-binding site within the membrane bilayer suggests a mechanistic role for this anion, perhaps in mediating protein–protein interactions. A subtle compression of the entire protein in this crystal form was interpreted as stemming from surface pressure effects within the stacked lipidic bilayers. It remains to be seen if this phenomenon proves general to high-resolution X-ray structures determined from lipid-rich crystals.

Materials and Methods

Purification and crystallisation of reaction centre from *Rhodobacter sphaeroides*

Photosynthetic reaction centres from *R. sphaeroides* (strain R26) were prepared to a high purity of $A_{280}/A_{800} < 1.2$ as described.[56] Crystals were grown using the lipidic cubic phase crystallisation method described by Chiu *et al.*[37] in which monoolein (NuChek Prep., Inc.) and 25 mg/ml of protein solution (in 10 mM Tris (pH 8.0), 1 mM EDTA, 0.1% (w/v) *N*,*N*-dimethyldodecylamine-*N*-oxide (LDAO) were mixed 60:40 (w/w) until transparent, non-birefringent and solid cubic phase was formed. The cubic phase and precipitant (1:4 ratio) were mixed by centrifugation in a glass

tube to the following final concentrations: 2.0 mg/ml of protein, 12% (w/v) monoolein, 14.4% (w/v) Jeffamine M-600, 0.8 M Hepes (pH 7.5), 0.56 M $(NH_4)_2SO_4$, ~0.008% LDAO. Plate-like crystals of about 0.05 mm × 0.05 mm × 0.02 mm were grown in three days at room temperature. These crystals were flash-frozen in liquid nitrogen without the addition of cryo-protectant.

Data collection and processing

Single crystal X-ray data were collected at 100K with an ADSC Q4 CCD detector at ID14-EH2 of the ESRF ($\lambda = 0.933$ Å). The oscillation range per image was 0.25°. Data were indexed and integrated with MOSFLM 6.2 and scaled with SCALA 2.7.5 of the CCP4 program suite.[57] The crystals belong to space group $P4_22_12$ with unit cell dimensions of $a = b = 100.0$ Å, and $c = 237.2$ Å. Subsequent data processing was carried out using programs in the CCP4 program suite.[57] Data statistics are summarized in Table 1.

Molecular replacement

The structure was solved by molecular replacement using the program AMoRe.[58] The starting coordinates were taken from the detergent-based crystal structure (Protein Data Bank entry 1aij, first NCS molecule)[7] and included the protein moiety only. The rotational search in the resolution range 8–3 Å resulted in a single peak far above the noise level. The translational search assuming the space group $P4_22_12$ produced the highest peak. After rigid body refinement in AmoRe, the correlation coefficient was 58.7 with an R-factor of 44.2%.

Model building and refinement

The model was improved systematically through iterative cycles of crystallographic refinement using the program CNS 1.1,[59] and manual rebuilding by means of O.[60] The model was checked by cross-validated SigmaA weighted electron density maps[61] calculated with both $2mF_o - DF_c$ and $mF_o - DF_c$ coefficients. Before any manual intervention, all models were subjected to one round of initial refinement by both simulated annealing and conjugate gradient minimization methods. All refinements were performed using an amplitude-based maximum likelihood target. Overall B-factor and bulk solvent corrections were applied. A random selection of approximately 5% of the data (test set) was assigned for calculation of the free R-factor,[62] and was not included in the refinement.

Quality check and analysis of the final model

The quality and stereochemistry of the model were monitored during the refinement with PROCHECK[63] and WHATCHECK.[64] ESCET 0.3[53] was used to identify the conformationally invariant regions of the protein. For the conformational analysis, eight high-quality (better than 2.8 Å resolution), detergent-based crystal structure was selected from three different space groups to minimize the influence of crystal packing on the analysis. A model based on the B-factors and quality of the structure was used to estimate the error for the atomic coordinates.[65] The rigid regions were then used to superimpose the detergent and lipid-based crystal structures. The least-squares fitting of C^α atoms in the rigid regions was performed using LSQKAB.[66] The Figures were generated with the combination of Bobscript,[67] POVscript + ,[68] Swiss PDB Viewer[69] and POV-RAY†.

Protein Data Bank accession number

The crystallographic data and the refined model have been deposited at the Protein Data Bank with accession code 1ogv.

Acknowledgements

We thank Eva Pebay-Peyroula, Pia Wadsten and Sven Engström for discussions. We thankfully acknowledge the support from synchrotron beamlines: Maxlab-II 711, ESRF ID-13, ID-14-EH1 and EH2, and SLS PX. This work was supported by Swedish Science Research Council (V.R.), SWEGENE, the Swedish Strategic Research Foundation (SSF), the European Commission Improving Human Potential Programme, the European Union-BIOTECH, and the Howard Hughes Medical Institute.

References

1. Deisenhofer, J., Epp, O., Miki, K., Huber, R. & Michel, H. (1984). X-ray structure analysis of a membrane protein complex. Electron density map at 3 Å resolution and a model of the chromophores of the photosynthetic reaction center from *Rhodopseudomonas viridis*. *J. Mol. Biol.* **180**, 385–398.
2. Allen, J. P., Feher, G., Yeates, T. O., Komiya, H. & Rees, D. C. (1987). Structure of the reaction center from *Rhodobacter sphaeroides* R-26: the cofactors. *Proc. Natl Acad. Sci. USA*, **84**, 5730–5734.
3. McAuley, K. E., Fyfe, P. K., Ridge, J. P., Isaacs, N. W., Cogdell, R. J. & Jones, M. R. (1999). Structural details of an interaction between cardiolipin and an integral membrane protein. *Proc. Natl Acad. Sci. USA*, **96**, 14706–14711.
4. Axelrod, H. L., Abresch, E. C., Paddock, M. L., Okamura, M. Y. & Feher, G. (2000). Determination of the binding sites of the proton transfer inhibitors Cd^{2+} and Zn^{2+} in bacterial reaction centers. *Proc. Natl Acad. Sci. USA*, **97**, 1542–1547.
5. Kuglstatter, A., Ermler, U., Michel, H., Baciou, L. & Fritzsch, G. (2001). X-ray structure analyses of photosynthetic reaction center variants from *Rhodobacter sphaeroides*: structural changes induced by point mutations at position L209 modulate electron and proton transfer. *Biochemistry*, **40**, 4253–4260.
6. Camara-Artigas, A., Brune, D. & Allen, J. P. (2002). Interactions between lipids and bacterial reaction centers determined by protein crystallography. *Proc. Natl Acad. Sci. USA*, **99**, 11055–11060.
7. Stowell, M. H., McPhillips, T. M., Rees, D. C., Soltis, S. M., Abresch, E. & Feher, G. (1997). Light-induced structural changes in photosynthetic reaction center: implications for mechanism of electron–proton transfer. *Science*, **276**, 812–816.

† http://www.povray.org

8. Buchanan, S. K., Fritzsch, G., Ermler, U. & Michel, H. (1993). New crystal form of the photosynthetic reaction centre from *Rhodobacter sphaeroides* of improved diffraction quality. *J. Mol. Biol.* **230**, 1311–1314.
9. Axelrod, H. L., Abresch, E. C., Okamura, M. Y., Yeh, A. P., Rees, D. C. & Feher, G. (2002). X-ray structure determination of the cytochrome c_2: reaction center electron transfer complex from *Rhodobacter sphaeroides*. *J. Mol. Biol.* **319**, 501–515.
10. Fritzsch, G., Koepke, J., Diem, R., Kuglstatter, A. & Baciou, L. (2002). Charge separation induces conformational changes in the photosynthetic reaction centre of purple bacteria. *Acta Crystallog. sect. D*, **58**, 1660–1663.
11. Lancaster, C. R., Bibikova, M. V., Sabatino, P., Oesterhelt, D. & Michel, H. (2000). Structural basis of the drastically increased initial electron transfer rate in the reaction center from a *Rhodopseudomonas viridis* mutant described at 2.00-Å resolution. *J. Biol. Chem.* **275**, 39364–39368.
12. Jordan, P., Fromme, P., Witt, H. T., Klukas, O., Saenger, W. & Krauss, N. (2001). Three-dimensional structure of cyanobacterial photosystem I at 2.5 Å resolution. *Nature*, **411**, 909–917.
13. Zouni, A., Witt, H., Kern, J., Fromme, P., Krauss, N., Saenger, W. & Orth, P. (2001). Crystal structure of photosystem II from *Synechococcus elongatus* at 3.8 Å resolution. *Nature*, **409**, 739–743.
14. Kuhlbrandt, W. (2001). Structural biology. Chlorophylls galore. *Nature*, **411**, 896–897. see also p. 899.
15. Prince, R. C. & Dutton, P. L. (1975). A kinetic completion of the cyclic photosynthetic electron pathway of *Rhodopseudomonas sphaeroides*: cytochrome *b*–cytochrome *c*2 oxidation–reduction. *Biochim. Biophys. Acta*, **387**, 609–613.
16. Henderson, R. & Unwin, P. N. (1975). Three-dimensional model of purple membrane obtained by electron microscopy. *Nature*, **257**, 28–32.
17. Henderson, R., Baldwin, J. M., Ceska, T. A., Zemlin, F., Beckmann, E. & Downing, K. H. (1990). Model for the structure of bacteriorhodopsin based on high-resolution electron cryo-microscopy. *J. Mol. Biol.* **213**, 899–929.
18. Essen, L., Siegert, R., Lehmann, W. D. & Oesterhelt, D. (1998). Lipid patches in membrane protein oligomers: crystal structure of the bacteriorhodopsin–lipid complex. *Proc. Natl Acad. Sci. USA*, **95**, 11673–11678.
19. Michel, H. & Oesterhelt, D. (1980). Three-dimensional crystals of membrane proteins: bacteriorhodopsin. *Proc. Natl Acad. Sci. USA*, **77**, 1283–1285.
20. Landau, E. M. & Rosenbusch, J. P. (1996). Lipidic cubic phases: a novel concept for the crystallization of membrane proteins. *Proc. Natl Acad. Sci. USA*, **93**, 14532–14535.
21. Luecke, H., Schobert, B., Richter, H. T., Cartailler, J. P. & Lanyi, J. K. (1999). Structure of bacteriorhodopsin at 1.55 Å resolution. *J. Mol. Biol.* **291**, 899–911.
22. Belrhali, H., Nollert, P., Royant, A., Menzel, C., Rosenbusch, J. P., Landau, E. M. & Pebay-Peyroula, E. (1999). Protein, lipid and water organization in bacteriorhodopsin crystals: a molecular view of the purple membrane at 1.9 Å resolution. *Struct. Fold Des.* **7**, 909–917.
23. Edman, K., Nollert, P., Royant, A., Belrhali, H., Pebay-Peyroula, E., Hajdu, J. *et al.* (1999). High-resolution X-ray structure of an early intermediate in the bacteriorhodopsin photocycle. *Nature*, **401**, 822–826.
24. Royant, A., Nollert, P., Edman, K., Neutze, R., Landau, E. M., Pebay-Peyroula, E. & Navarro, J. (2001). X-ray structure of sensory rhodopsin II at 2.1-Å resolution. *Proc. Natl Acad. Sci. USA*, **98**, 10131–10136.
25. Royant, A., Edman, K., Ursby, T., Pebay-Peyroula, E., Landau, E. M. & Neutze, R. (2000). Helix deformation is coupled to vectorial proton transport in the photocycle of bacteriorhodopsin. *Nature*, **406**, 645–648.
26. Luecke, H. (2000). Atomic resolution structures of bacteriorhodopsin photocycle intermediates: the role of discrete water molecules in the function of this light-driven ion pump. *Biochim. Biophys. Acta*, **1460**, 133–156.
27. Luecke, H., Schobert, B., Richter, H. T., Cartailler, J. P. & Lanyi, J. K. (1999). Structural changes in bacteriorhodopsin during ion transport at 2 angstrom resolution. *Science*, **286**, 255–261.
28. Facciotti, M. T., Rouhani, S., Burkard, F. T., Betancourt, F. M., Downing, K. H., Rose, R. B. *et al.* (2001). Structure of an early intermediate in the M-state phase of the bacteriorhodopsin photocycle. *Biophys. J.* **81**, 3442–3455.
29. Sass, H. J., Buldt, G., Gessenich, R., Hehn, D., Neff, D., Schlesinger, R. *et al.* (2000). Structural alterations for proton translocation in the M state of wild-type bacteriorhodopsin. *Nature*, **406**, 649–653.
30. Vonck, J. (2000). Structure of the bacteriorhodopsin mutant F219L N intermediate revealed by electron crystallography. *EMBO J.* **19**, 2152–2160.
31. Subramaniam, S., Lindahl, I., Bullough, P., Faruqi, A. R., Tittor, J., Oesterhelt, D. *et al.* (1999). Protein conformational changes in the bacteriorhodopsin photocycle. *J. Mol. Biol.* **287**, 145–161.
32. Neutze, R., Pebay-Peyroula, E., Edman, K., Royant, A., Navarro, J. & Landau, E. M. (2002). Bacteriorhodopsin: a high-resolution structural view of vectorial proton transport. *Biochim. Biophys. Acta*, **1565**, 144–167.
33. Kolbe, M., Besir, H., Essen, L. O. & Oesterhelt, D. (2000). Structure of the light-driven chloride pump halorhodopsin at 1.8 Å resolution. *Science*, **288**, 1390–1396.
34. Luecke, H., Schobert, B., Lanyi, J. K., Spudich, E. N. & Spudich, J. L. (2001). Crystal structure of sensory rhodopsin II at 2.4 angstroms: insights into color tuning and transducer interaction. *Science*, **293**, 1499–1503.
35. Edman, K., Royant, A., Nollert, P., Maxwell, C. A., Pebay-Peyroula, E., Navarro, J. *et al.* (2002). Early structural rearrangements in the photocycle of an integral membrane sensory receptor. *Structure (Camb.)*, **10**, 473–482.
36. Gordeliy, V. I., Labahn, J., Moukhametzianov, R., Efremov, R., Granzin, J., Schlesinger, R. *et al.* (2002). Molecular basis of transmembrane signalling by sensory rhodopsin II–transducer complex. *Nature*, **419**, 484–487.
37. Chiu, M. L., Nollert, P., Loewen, M. C., Belrhali, H., Pebay-Peyroula, E., Rosenbusch, J. P. & Landau, E. M. (2000). Crystallization *in cubo*: general applicability to membrane proteins. *Acta Crystallog. sect. D*, **56**, 781–784.
38. Pebay-Peyroula, E., Rummel, G., Rosenbusch, J. P. & Landau, E. M. (1997). X-ray structure of bacteriorhodopsin at 2.5 angstroms from microcrystals grown in lipidic cubic phases. *Science*, **277**, 1676–1681.
39. Luecke, H., Richter, H. T. & Lanyi, J. K. (1998). Proton transfer pathways in bacteriorhodopsin at 2.3 angstroms resolution. *Science*, **280**, 1934–1937.

40. Nollert, P., Qiu, H., Caffrey, M., Rosenbusch, J. P. & Landau, E. M. (2001). Molecular mechanism for the crystallization of bacteriorhodopsin in lipidic cubic phases. *FEBS Letters*, **504**, 179–186.
41. Pape, E. H., Menke, W., Weick, D. & Hosermann, R. (1974). Small angle X-ray scattering of the thylakoid membranes of *Rhodopseudomonas speroides* in aqueous suspensions. *Biophys. J.* **14**, 221–232.
42. Marinetti, G. V. & Cattieu, K. (1981). Lipid analysis of cells and chromatophores of *Rhodopseudomonas sphaeroides*. *Chem. Phys. Lipids*, **28**, 241–251.
43. Yeates, T. O., Komiya, H., Rees, D. C., Allen, J. P. & Feher, G. (1987). Structure of the reaction center from *Rhodobacter sphaeroides* R-26—membrane–protein interactions. *Proc. Natl Acad. Sci. USA*, **84**, 6438–6442.
44. Overfield, R. E. & Wraight, C. A. (1980). Oxidation of cytochromes *c* and *c*2 by bacterial photosynthetic reaction centers in phospholipid vesicles. 2. Studies with negative membranes. *Biochemistry*, **19**, 3328–3334.
45. Morrison, L., Runquist, J. & Loach, P. (1977). Ubiquinone and photochemical activity in *Rhodospirillum rubrum*. *Photochem. Photobiol.* **25**, 73–84.
46. Vermeglio, A., Joliot, P. & Joliot, A. (1993). The rate of cytochrome *c*(2) photooxidation reflects the subcellular-distribution of reaction centers in *Rhodobacter sphaeroides* Ga cells. *Biochim. Biophys. Acta*, **1183**, 352–360.
47. Francia, F., Wang, J., Venturoli, G., Melandri, B. A., Barz, W. P. & Oesterhelt, D. (1999). The reaction center–LH1 antenna complex of *Rhodobacter sphaeroides* contains one PufX molecule which is involved in dimerization of this complex. *Biochemistry*, **38**, 6834–6845.
48. Loach, P. A. (2000). Supramolecular complexes in photosynthetic bacteria. *Proc. Natl Acad. Sci. USA*, **97**, 5016–5018.
49. Wakeham, M. C., Sessions, R. B., Jones, M. R. & Fyfe, P. K. (2001). Is there a conserved interaction between cardiolipin and the type II bacterial reaction center? *Biophys. J.* **80**, 1395–1405.
50. Lancaster, C. R. & Michel, H. (1997). The coupling of light-induced electron transfer and proton uptake as derived from crystal structures of reaction centres from *Rhodopseudomonas viridis* modified at the binding site of the secondary quinone, QB. *Structure*, **5**, 1339–1359.
51. Johnson, E. T. & Parson, W. W. (2002). Electrostatic interactions in an integral membrane protein. *Biochemistry*, **41**, 6483–6494.
52. Vermeglio, A. & Joliot, P. (2002). Supramolecular organisation of the photosynthetic chain in anoxygenic bacteria. *Biochim. Biophys. Acta*, **1555**, 60–64.
53. Schneider, T. R. (2002). A genetic algorithm for the identification of conformationally invariant regions in protein molecules. *Acta Crystallog. sect. D*, **58**, 195–208.
54. Facci, P., Erokhin, V., Paddeu, S. & Nicolini, C. (1998). Surface pressure induced structural effects in photosynthetic reaction center Langmuir–Blodgett films. *Langmuir*, **14**, 193–198.
55. Erokhin, V., Facci, P., Kononenko, A., Radicchi, G. & Nicolini, C. (1996). On the role of molecular close packing on the protein thermal stability. *Thin Solid Films*, **285**, 805–808.
56. Feher, G. & Okamura, M. Y. (1978). Chemical composition and properties of reaction centers. In *The Photosynthetic Bacteria* (Clayton, R. K. & Sistrom, W. R., eds), pp. 349–386, Plenum Press, New York.
57. Collaborative Computational Project, Number 4 (1994). The CCP4 suite: programs for protein crystallography. *Acta Crystallog. sect. D*, **50**, 760–763.
58. Navaza, J. & Saludjian, P. (1997). AMoRe: an automated molecular replacement program package. *Methods Enzymol.* **276**, 581–594.
59. Brunger, A. T., Adams, P. D., Clore, G. M., DeLano, W. L., Gros, P., Grosse-Kunstleve, R. W. *et al.* (1998). Crystallography NMR system: a new software suite for macromolecular structure determination. *Acta Crystallog. sect. D*, **54**, 905–921.
60. Jones, T. A. & Kjeldgaard, M. (1997). Electron-density map interpretation. *Methods Enzymol.* **277**, 173–208.
61. Read, R. J. (1986). Improved Fourier coefficients for maps using phases from partial structures with errors. *Acta Crystallog. sect. A*, **42**, 140–149.
62. Brunger, A. T. (1992). Free *R* value: a novel statistical quantity for assessing the accuracy of crystal structures. *Nature*, **355**, 472–475.
63. Laskowski, R. A., MacArthur, M. W., Moss, D. S. & Thornton, J. M. (1993). PROCHECK: a program to check the stereochemical quality of protein structures. *J. Appl. Crystallog.*, **26**, 283–291.
64. Hooft, R. W., Vriend, G., Sander, C. & Abola, E. E. (1996). Errors in protein structures. *Nature*, **381**, 272.
65. Schneider, T. R. (2000). Objective comparison of protein structures: error-scaled difference distance matrices. *Acta Crystallog. sect. D*, **56**, 714–721.
66. Kabsch, W. (1976). A solution for the best rotation to relate two sets of vectors. *Acta Crystallog. sect. A*, **32**, 922–923.
67. Esnouf, R. M. (1997). An extensively modified version of MolScript that includes greatly enhanced coloring capabilities. *J. Mol. Graph. Model.* **15**, 112–113. see also pp. 132–134.
68. Fenn, T. D., Ringe, D. & Petsko, G. A. (2003). POVScript + a program for model and data visualization using persistence of vision ray-tracing. *J. Appl. Crystallog.* **36**, 944–947.
69. Guex, N. & Peitsch, M. C. (1997). SWISS-MODEL and the Swiss-PdbViewer: an environment for comparative protein modeling. *Electrophoresis*, **18**, 2714–2723.
70. Camara-Artigas, A., Magee, C. L., Williams, J. C. & Allen, J. P. (2001). Individual interactions influence the crystalline order for membrane proteins. *Acta Crystallog. sect. D*, **57**, 1281–1286.
71. Ridge, J. P., Fyfe, P. K., McAuley, K. E., van Brederode, M. E., Robert, B., van Grondelle, R. *et al.* (2000). An examination of how structural changes can affect the rate of electron transfer in a mutated bacterial photoreaction centre. *Biochem. J.* **3**, 567–578.
72. Ermler, U., Fritzsch, G., Buchanan, S. K. & Michel, H. (1994). Structure of the photosynthetic reaction centre from Rhodobacter sphaeroides at 2.65 Å resolution: cofactors and protein–cofactor interactions. *Structure*, **2**, 925–936.

Edited by D. Rees

(Received 19 March 2003; received in revised form 6 June 2003; accepted 9 June 2003)